Physical Insights into Light Interacting with Matter

Gas-phase Synthesis and Characterisation of the Methyl-2,2-dicyanoacetate Anion Using Photoelectron Imaging and Dipole-bound State Autodetachment

Cate S. Anstöter, and Jan R. R. Verlet

J. Phys. Chem. Lett., **Just Accepted Manuscript** • DOI: 10.1021/acs.jpclett.0c02036 • Publication Date (Web): 20 Jul 2020

Gas-phase Synthesis and Characterisation of the Methyl-2,2-dicyanoacetate Anion Using Photoelectron Imaging and Dipole-bound State Autodetachment

*Cate S. Anstöter**† and Jan R. R. Verlet*

Department of Chemistry, Durham University, Durham DH1 3LE, United Kingdom

† *Present Address: Department of Chemistry, Temple University, Philadelphia, PA, 19122, United States of America*

Abstract

The methyl-2,2-dicyanoacetate anion is synthesised in an electrospray ionisation source through a gas-phase reaction involving tetracyanoethylene and methanol. Photoelectron imaging is used to determine the isomeric form of the product. The photoelectron spectra and angular distributions are only consistent with a single isomer. Additionally, mode-specific vibrational autodetachment is observed. This can be correlated with the emission from a photoexcited dipole-bound state by considering the IR spectrum of the neutral molecule, adding further confirmation of the isomeric form and providing a binding energy of the dipole-bound state. Our experiments show how conventional photoelectron imaging can be used to determine detailed information about gas-phase reaction products.

*csanstoter@gmail.com

TOC GRAPHICS

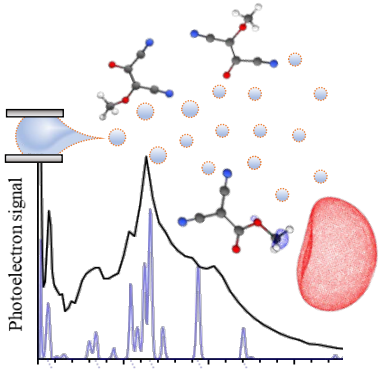

KEYWORDS Anion photoelectron spectroscopy, non-valence state, electrospray ionization, Dyson orbital, photoelectron angular distributions, autodetachment

Gas-phase ion chemistry has been extensively used to produce a wide range of species that would be difficult to make using traditional synthetic methods. For example, exotic anions can be made *in situ* in supersonic expansions, in the electrospray ionisation (ESI) processes, or by collision-induced dissociation.[1–4] Mass-spectrometry is then used as a measure of the reaction products, which are often generated by careful design of the reactants and conditions. Some products are also produced by accident. Regardless of the intentions, isomeric forms of the intended products can commonly be formed, especially in energetic reactions such as in plasmas or collision-induced dissociation. To identify isomers requires spectroscopic techniques that are coupled to mass-spectrometry. Examples include: infrared spectroscopy (either multiphoton[5,6] or messenger-tagged[7,8]), double-resonance (hole-burning) methods,[9] or photoelectron spectroscopy.[10] For the latter, high-resolution variants are particularly well suited to provide definitive assignments.[11,12] Here, we show that even at relatively low resolution, isomeric identification is possible by exploiting the additional information offered by the photoelectron angular distributions and resonance-enhanced excitation to a non-valence state. These added measures, when combined with calculations, provide a definitive assignment of the isomer produced of an ESI-synthesised organic anion.

Photoelectron spectroscopy has been used for many decades to determine geometric and electronic structure of gas-phase species. In particular, anion photoelectron spectroscopy[13–15] is easily coupled to mass-spectrometry as the latter can isolate a single m/z ion to be investigated. Electron emission can generate the neutral ground state and therefore, provide detailed information about the neutral including its electron affinity and geometric parameters (*i.e.,* vibrational frequencies). Particularly impressive has been the development of cryogenic slow electron velocity map imaging,[10,16] where the resolution can be as good as a few wavenumbers, which is easily sufficient to distinguish isomers. However, such methods also come with experimental complications as they require cooling of the ions to

remove spectral congestion and the electron imaging is very sensitive to stray electric fields because the electrons have very low kinetic energy. However, conventional photoelectron imaging can also offer added information that is often disregarded. Specifically, photoelectron angular distributions provide a measure of the molecular orbital from which the electron was detached,[17,18] but this orbital is of course also sensitive to the geometry of the anion.[19–21] Additionally, photodetachment near the detachment threshold can lead to the excitation of vibrational resonances of non-valence states, either directly[16,22] or indirectly,[23–26] which yields structure in low energy electron emission that can be correlated with vibrational modes of the final neutral state, thus offering an additional measure of structure. Here, we exploit this additional information to determine which of a number of possible isomers are formed in a gas-phase reaction.

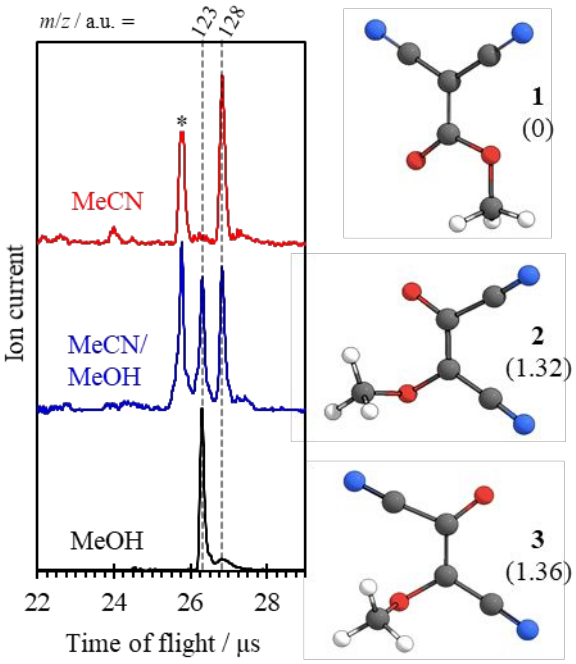

Figure 1: Time-of-flight mass spectrum of TCNE (m/z = 128) following negative mode ESI from different solutions. In the presence of MeOH, a new product (m/z = 123) is seen, with the three possible isomers shown, including their relative energies in parenthesis in eV. The peak marked with an asterisk is not identified.

We set out initially to study the tetracyanoethylene (TCNE) anion. Figure 1 shows the time-of-flight mass spectrum following the ESI of a solution of TCNE dissolved in: MeCN, a MeCN:MeOH (1:1) mixture, or MeOH. The mass peak associated with $TCNE^-$ (m/z = 128 amu) is clearly present when sprayed in pure MeCN, with an additional peak that we have not assigned indicated by the asterisks. In the MeCN:MeOH mixture, a new peak is present, while in methanol, only a single dominant peak at m/z = 123 amu is seen. Given the reactants present, the mass of this anion suggests that it arises from the loss of two cyano-groups from TCNE and their substitution with and oxygen and a methoxy-group, presumably forming HCN as a by-product. Apparently, the reaction is very facile and no other product anions are observed.

While the mass provides a chemical formula for the ESI-synthesised compound, $C_5N_2H_3O_2^-$, three isomeric forms of the product are possible. The two cyano-groups can be substituted on a single carbon or one on each carbon, with the latter having a *cis* and *trans* isomer. These three possible isomers for the methyl-dicyanoacetate anion ($MDCA^-$), isomers **1**, **2**, and **3**, respectively, are shown in Figure 1. Figure 2(a) shows the photoelectron spectra taken over a range of photon energies ($3.70 < h\nu < 4.35$ eV) with Figure 2(b) showing the specific spectrum at $h\nu$ = 4.20 eV. From the latter, the adiabatic detachment energy (ADE) and vertical detachment energy (VDE) of $MDCA^-$ were determined 3.60±0.10 eV and 3.77±0.10 eV, respectively. Figure 2(c) shows the measured anisotropy associated with the photoelectron emission, which is quantified using the anisotropy parameter, β_2.[27] It has been determined by averaging the β_2 values across the highest intensity region of the direct detachment peak.

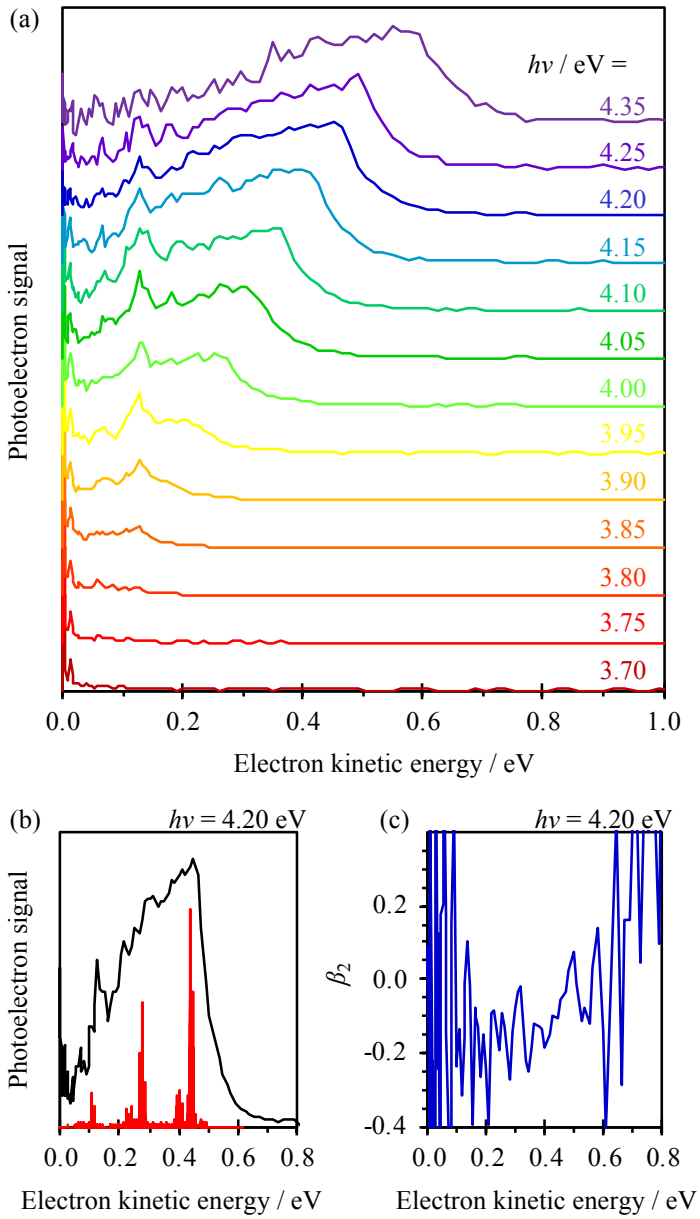

Figure 2: (a) Photoelectron spectra of $DCNE^-$ taken at a range of photon energies as indicated. Vertical dashed lines highlight structure at low kinetic energy in spectra. (b) Representative photoelectron spectrum at $h\nu = 4.20$ eV with corresponding β_2 spectrum in (c). The modelled photodetachment spectrum (red sticks) is shown alongside the experimental spectrum (black line) in (b).

The kinetic energy of the dominant peak at $h\nu = 4.35$ eV in Figure 2(a) decreases proportional to the decrease in photon energy and ultimately can no longer be distinguished for $h\nu < 3.80$ eV. This feature arises from direct detachment of $MDCA^-$ leaving the neutral in

its ground electronic state. However, in addition to this direct detachment channel, there are distinct peaks apparent at low kinetic energy that do not shift in kinetic energy despite the varying photon energy. These are highlighted by vertical dashed lines and appear at kinetic energies of 14, 66 and 126 meV. Interestingly, the peaks do not appear all at once, with the higher lying peaks becoming apparent at higher photon energies. For example, the spectrum at $h\nu$ = 3.70 eV shows only evidence of the peak at 14 meV. As the photon energy increases, we begin to see electron emission occur from the second (66 meV) and third (126 meV) peaks at $h\nu$ = 3.75 and 3.80 eV, respectively. These channels remain visible at most $h\nu$ but disappear at higher $h\nu$, with the 14 meV peak becoming indistinguishable at $h\nu \sim 4.20$ eV, followed by the peak at 66 meV at $h\nu \sim 4.25$ eV and finally the peak at 124 meV at $h\nu \sim 4.35$ eV. Hence, there is a limited photon energy window over which the specific low-energy peaks are observed.

We aide the interpretation of the experimental data using electronic structure calculations. DFT calculations predict that the isomer formed from substitution of the cyano-groups on the same carbon, methyl-2,2-dicyanoacetate anion (isomer **1**, Figure 1), is the most energetically stable by more than 1.3 eV. Hence, even at 300 K, we anticipate that the isomer **1** will be the only isomer present in the ion packet. The preferential formation of isomer **1** is in agreement with a multistep cobalt-catalysed synthesis of MDCA from TCNE.[28] The ADE and VDE calculated at the CAM-B3LYP/aug-cc-pVDZ level predict values of 3.76 and 3.91 eV, respectively. A higher-level EOM-IP-CCSD calculation predicts a VDE of 3.81 eV. DFT calculations of isomers **2** and **3** yield values for the ADE and VDE of 3.27 and 3.72 eV, and 3.15 and 3.69 eV, respectively. The experimental values of 3.60±0.10 and 3.77±0.10 eV are closest to that of isomer **1**. However, the added information in Figure 2 can be exploited to be much more certain of this assignment.

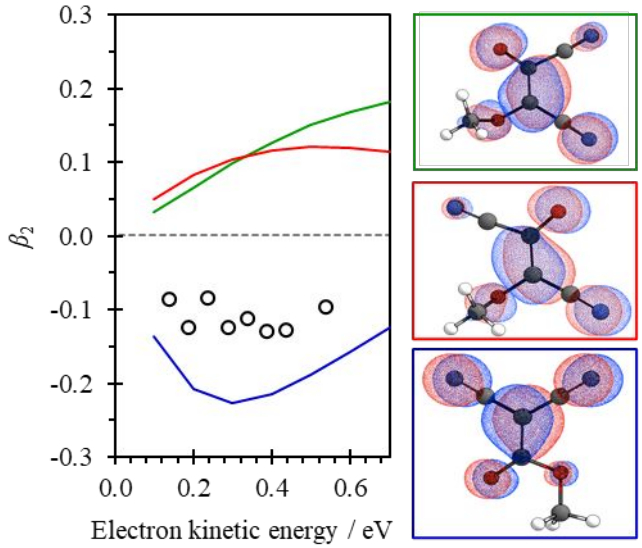

Figure 3: β_2 determined at a number of different *hv* from the experimental photoelectron images (open circles) together with calculated β_2 from the Dyson orbital for the three different isomers shown.

For direct detachment, the photoelectron angular distributions are dictated by the molecular orbital from which the electron is removed (the Dyson orbital). From Figure 2(b), over the kinetic energy range in which there is meaningful photoelectron signal, the β_2 values are broadly negative. Based on symmetry arguments, negative β_2 values can be qualitatively interpreted to arise from photodetachment of a molecular orbital with π-character.[18] The photoelectron angular distributions can also be quantitatively predicted using the Dyson orbital approach.[29,30] Figure 3 shows the calculated β_2 parameters as a function of kinetic energy of the electron for the different isomers. Isomers **2** and **3** have positive values of β_2 over the kinetic energy range probed in the experiment. In contrast, isomer **1** shows negative β_2 values in reasonable agreement with the experimental trends in Figure 2(c). Hence, the photoelectron angular distributions can serve as a sensitive diagnostic of structure. This is

because the different substitution positions cause subtle changes to the electronic structure that directly determine the Dyson orbital. However, from simple inspection of the Dyson orbitals in Figure 3, it is not immediately obvious why these differences are so apparent because all the isomers have Dyson orbitals of predominantly π-character. In the case of $MDCA^-$, there are geometric arguments that come into play. Only isomer **1** has a fully planar geometry; for isomers **2** and **3**, the methoxy-groups are rotated out of the π-plane. We have previously shown how the photoelectron angular distributions are sensitive to such subtle geometric differences, which cause partial s- or σ-mixing into the Dyson orbital.[19,21] While the qualitative agreement with isomer **1** is good, there are quantitative discrepancies between the measured and computed angular distributions. This may be due to the finite temperature of the ions, the neglect of a long-range (dipole-electron) interaction in the model, and because of the ability for the methyl group to undergo essentially free rotation.

Finally, we consider the narrow peaks that are apparent at low energy in Figure 2(a). Structured peaks at low kinetic energy have been observed in a number of studies and a mechanism has recently been put forward to explain their structure.[23,26] Specifically, these peaks have been associated with the presence of non-valence states that become populated and then undergo mode-specific vibrational autodetachment. For such a process to be operable in $MDCA^-$, the anion must possess a non-valence state. The most common non-valence state is a dipole-bound state (DBS) in which the excess electron is bound by a large (>2.5 D) permanent dipole moment of the neutral core.[14,31] The calculated dipole-moment for isomer **1** is 4.7 D, suggesting that a DBS will exist.

In several previous studies, where mode-specific vibrational autodetachment was observed,[22,24,26] the non-valence state was populated indirectly and was preceded by the excitation to valence resonances of the anion. However, for isomer **1**, our calculations show that there are no excited states or resonances in the experimental range probed. The lowest-lying resonance has a calculated vertical excitation energy of 4.35 eV and has a very small oscillator strength (8.5×10^{-5}). Hence, the observation of the vibronic structure at photon energies as low as $h\nu = 3.80$ eV is inconsistent with the calculated energy of the valence resonances. Instead, the DBS can be directly excited. Even though direct excitation of a DBS may have a low oscillator strength because of the poor overlap between valence and non-valence orbitals, resonant excitation has been clearly observed in many cases[32–36] and, for example, exploited as an accurate probe for the structure of neutral ground states by Wang and coworkers.[23,37]

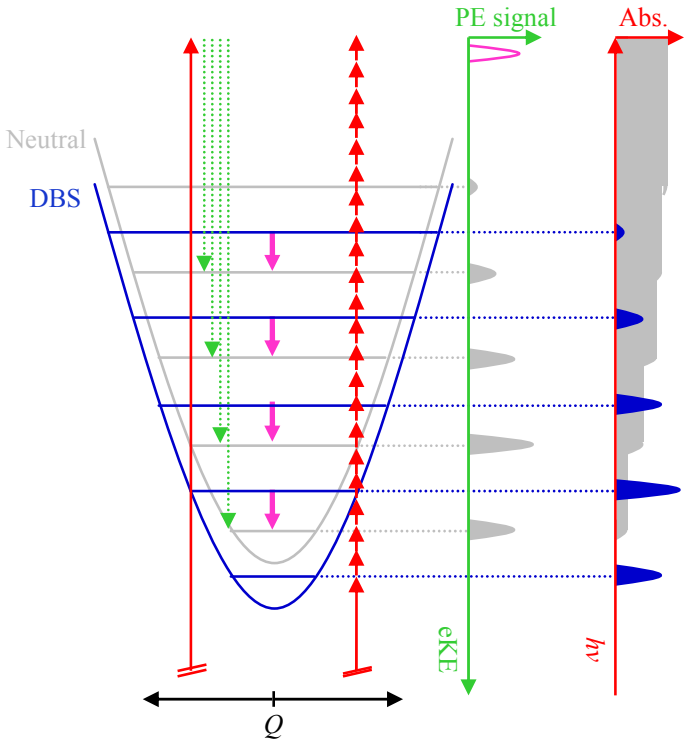

Figure 4: Schematic of processes involved for a single (harmonic) vibrational mode, *Q*. Upward red arrows represent a photon; downward green dashed arrows photoelectrons; and downward pink arrows electron produced by vibrational autodetachment from a DBS (blue) to the neutral ground state (grey). The sketched grey spectrum represents the photoelectron spectrum, while the sketched blue spectrum represents the absorption cross section of the

vibrational levels from the ground anion state (not shown) to the DBS and the contribution of the continuum (grey shaded). Note that the Franck-Condon profiles of the photoelectron spectrum and the absorption spectrum are the same. The photoelectron spectrum shows where the autodetachment would be if the DBS was excited.

The mode-specificity of the vibrational autodetachment from a non-valence state is rooted the nature of the electron binding. The potential energy surface of a non-valence state and of the corresponding neutral final state are essentially parallel, especially near the minimum energy structure, shown schematically in Figure 4. As a consequence, vibrational autodetachment of the DBS to the corresponding levels of the neutral tend to obey a $\Delta v = -1$ propensity rule.[38] However, not all modes autodetach equally. In a simple picture, it is the vibrational modes that are strongly coupled to the non-valence state binding that facilitate electron emission. For a DBS, these are the modes that strongly modulate the permanent dipole-moment of the neutral core. That is to say, excited IR-active modes of the neutral effectively "shake off" the excess non-valence electron. In combination with the $\Delta v = -1$ propensity rule, this mode-specific autodetachment mechanism will lead to peaks in the photoelectron spectrum corresponding to IR-active modes that are red-shifted by the binding energy of the DBS.[26]

Figure 5(a) shows the computed DBS orbital, along with the dipole moment vector, for isomer **1** in its neutral minimum energy geometry. The DBS is calculated to be bound by 30 meV. Figure 5(b) show a comparison of the IR spectrum of isomer **1** with the low-energy structured photoelectron emission. Specifically, the IR spectrum is shown in Figure 5(c) and correlated to features in the low energy emission channel for a spectrum taken at $h\nu = 3.90$ eV, which is shown in Figure 5(b). When a red-shift of ~35 meV is applied to the calculated IR spectrum, most of computed IR modes correlate with features in the photoelectron spectrum. To emphasise this correlation, we have reproduced the offset IR spectrum and superimposed it onto the photoelectron spectrum (Figure 5(b)). In this comparison, the IR

spectrum has been scaled by the inverse of the electron kinetic energy to account for the denominator in the expression for vibrational autodetachment from a non-valence state derived by Simons.[38] Note that, even with this scaling, the intensities are likely to be inaccurate. However, as MDCA does not have symmetry restrictions governing non-adiabatic coupling of the DBS and neutral ground state, in principle any IR active modes may lead to non-zero couplings between the DBS and the continuum. The offset in energy between the photoelectron spectra and the IR spectrum corresponds to the offset in energy between the potential energy surfaces of the DBS and the neutral ground state. This is equivalent to the binding energy of the DBS, which is found to be ~35 meV and is in good agreement with the computed binding energy of 30 meV. The scaled IR fit provides excellent agreement with the low energy electron structure in Figure 5(b), the only feature that appears to be unaccounted for by the fit is a shoulder at eKE ~ 0.225 eV. This shoulder corresponds to the onset of the direct detachment channel.

The mode-specific autodetachment is only observed over a limited photon energy range. This range corresponds to the Franck-Condon (and Boltzmann) factors associated with excitation to the DBS. Specifically, because the DBS and neutral final states are parallel, we anticipate a similar Franck-Condon profile for both excitation to the DBS and the photoelectron spectrum from the anion ground state, as shown schematically in Figure 4. Hence, the broad photoelectron spectrum as indicated by the direct detachment (Figure 2(a)) has the autodetachment of the specific IR-active modes superimposed on it. Once the direct detachment leads only to photoelectrons with significant kinetic energy, we do not expect to be able to photoexcite the DBS. This argument is fully consistent with the data in Figure 2(a) that shows how the vibrational levels appear only when sufficient photon energy is present to directly excite them and that they subsequently disappear because the photon energy is above those vibrational levels of the DBS for which there is good Franck-Condon overlap.

For completeness, we also considered isomers **2** and **3**. Both have sufficiently large dipole moments to host a DBS with binding energies that were calculated to be 54 and 52 meV for isomer **2** and **3**, respectively. The shifted IR spectra for all isomers are provided in the Supporting Information. It should be noted that the neutral equilibrium geometries for isomers **2** and **3** are planar, while the anion equilibrium geometries are bent (as evidenced by the photoelectron angular distributions, Figure 3), and as such there is a very large displacement between the anion and neutral ground state potential energy surfaces, leading to a very broad Franck-Condon window, which is inconsistent with the observations. Moreover, the shifted IR spectra for these isomers does not provide good agreement with the low energy structure seen experimentally.

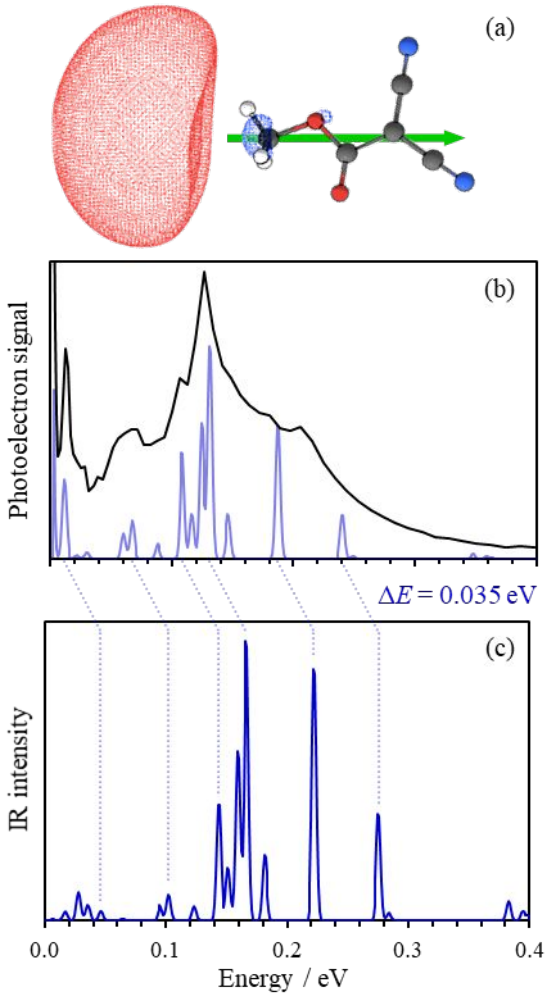

Figure 5: (a) Computed dipole moment and dipole-bound state orbital of isomer **1**. (b) Photoelectron spectrum taken at $h\nu$ = 3.90 eV (black line). (c) Calculated IR spectrum (blue line). Applying a $\Delta E = -35$ meV shift to the IR spectrum (light blue lines) leads to a good correlation between IR modes and mode-specific autodetachment peaks in the photoelectron spectrum. This correlation is shown by the scaled IR spectrum in (b).

The mechanism for low energy emission should be a general feature of anion photoelectron spectroscopy near threshold if the neutral has a sufficient dipole-moment (or multipole and correlation energy). Surprisingly, however, to the best of our knowledge, these features have not been explicitly observed or explained, except in the context of cryo-slow electron velocity map imaging (SEVI) experiments by Wang and coworkers.[16,23,39] There may be several reasons for this. Firstly, typical anion photoelectron spectroscopy is not performed near threshold because detachment cross sections are small and the entire Franck-Condon envelope may not be apparent. Secondly, it is only through 2D photoelectron spectroscopy that such peaks stand out because they do not shift with kinetic energy. Thirdly, resonant excitation cross sections to the DBS may be small compared to direct detachment. In the present case, we appear to have a relatively large excitation cross section for the DBS, which may be a consequence of the large-dipole moment that binds the DBS more strongly leading to better overlap between the valence and non-valence orbitals.

In conclusion, we have synthesised an organic molecule anion within an ESI source and have characterised the anion using photoelectron imaging. Three isomeric forms of the anion can in principle be produced and the photoelectron imaging offered: the vertical and adiabatic detachment energies; the photoelectron angular distributions; and the mode-specific vibrational autodetachment from a dipole-bound state. Based on these, an unambiguous assignment could be made, showing that photoelectron imaging can serve as a sensitive analytical tool.

Experimental

Were produced by ESI of ~1 mM solution of tetracyanoethylene (TCNE) in methanol and acetonitrile. The anions generated were introduced to vacuum by a capillary tube and guided along a series of differentially pumped regions by a series of ring-electrode ion guides to a terminated ion trap.[40] Anions were pulsed out of the trap into a colinear Wiley-McLaren time-of-flight (TOF) mass spectrometer.[41] Mass-selected anion packets were irradiated with light from a tunable nanosecond laser pulse generated by a Nd:YAG pumped OPO. Photodetached electrons were detected using a velocity map imaging (VMI) assembly.[42,43] The PE spectra and angular distributions (PADs) were extracted using polar onion peeling algorithm from raw VMI images.[44] The known atomic spectrum of I^- was used to calibrate PE spectra. PE spectra have experimental resolution of ~5%.

Computational

All geometric and energetic calculations were carried out using the QChem 5.0 computational package.[45] Initial calculations of the neutral and anion ground states geometries of three mass-degenerate isomers were optimized using CAM-B3LYP/aug-cc-pVDZ level of theory.[46,47] The geometries obtained were verified to be global minimum energy structures by vibrational analysis, the IR spectrum of the neutral isomer **1** was taken from this calculation and convoluted with a Gaussian with full width at half maximum of 3 meV. All energetics were corrected for zero-point energy. The photodetachment spectrum for isomer **1** was modelled at this level of theory using ezSpectrum 3.0, developed by Krylov and coworkers.[48]

Additional equations-of-motion ionisation potential coupled cluster singles and doubles (EOM-IP-CCSD)[29,49] calculations were used to obtain Dyson Orbitals. Dyson orbitals were used to model the direct detachment channels for the anion using ezDyson v4, developed by Krylov and co-workers.[50] Electronic excitation (EOM-EE-CCSD)

calculations[51] were performed to find the vertical excitation energies (VEEs) of the anion excited states.

The energy of the DBS was calculated using EOM-EA-CCSD and a custom basis set. The DBS binding energy calculations were performed through addition of a ghost atom to the centre of mass of the MP2/aug-cc-pVDZ re-optimised neutral isomer **1**. The neutral valence system was treated with the aug-cc-pVDZ basis set, and the non-valence DBS was treated through affixing very diffuse basis functions (6s6p6d) to the ghost atom. The coefficients of the diffuse basis functions were chosen to be even-tempered, in accordance with previous works.[31,52,53] The energy of the DBS for isomers **2** and **3** were also calculated using this method.

Acknowledgements

This work has been funded by the European Research Council (Grant number 306536).

References

(1) Froelicher, S. W.; Freiser, B. S.; Squires, R. R. The C3H5- Isomers . Experimental and Theoretical Studies of Gas Phase. **1986**, No. 18, 2853–2862.

(2) Graul, S. T.; Squires, R. R. On the Existence of Alkyl Carbanions in the Gas Phase. *J Am Chem Soc* **1988**, *110*, 607–608.

(3) DePuy, C. H.; Bierbaum, V. M.; Flippin, L. A.; Grabowski, J. J.; King, G. K.; Schmitt, R. J.; Sullivan, S. A. Gas-Phase Reactions of Anions with Substituted Silanes. *J. Am. Chem. Soc.* **1980**, *102* (15), 5012–5015. https://doi.org/10.1021/ja00535a031.

(4) Tian, Z.; Kass, S. R. Carbanions in the Gas Phase. *Chem. Rev.* **2013**, *113* (9), 6986–7010. https://doi.org/10.1021/cr4000896.

(5) Polfer, N. C. Infrared Multiple Photon Dissociation Spectroscopy of Trapped Ions. *Chem. Soc. Rev.* **2011**, *40* (5), 2211–2221. https://doi.org/10.1039/C0CS00171F.

(6) Oomens, J.; Sartakov, B. G.; Meijer, G.; von Helden, G. Gas-Phase Infrared Multiple Photon Dissociation Spectroscopy of Mass-Selected Molecular Ions. *Int. J. Mass Spectrom.* **2006**, *254* (1), 1–19. https://doi.org/10.1016/j.ijms.2006.05.009.

(7) Wolk, A. B.; Leavitt, C. M.; Garand, E.; Johnson, M. A. Cryogenic Ion Chemistry and Spectroscopy. *Acc. Chem. Res.* **2014**, *47* (1), 202–210. https://doi.org/10.1021/ar400125a.

(8) Dopfer, O.; Fujii, M. Probing Solvation Dynamics around Aromatic and Biological Molecules at the Single-Molecular Level. *Chem. Rev.* **2016**, *116* (9), 5432–5463. https://doi.org/10.1021/acs.chemrev.5b00610.

(9) Rizzo, T. R.; Stearns, J. A.; Boyarkin, O. V. Spectroscopic Studies of Cold, Gas-Phase Biomolecular Ions. *Int. Rev. Phys. Chem.* **2009**, *28* (3), 481–515. https://doi.org/10.1080/01442350903069931.

(10) Weichman, M. L.; Neumark, D. M. Slow Photoelectron Velocity-Map Imaging of Cryogenically Cooled Anions | Annual Review of Physical Chemistry. *Annu. Rev. Phys. Chem.* **2018**, *69*, 101–124. https://doi.org/10.1146/annurev-physchem-050317-020808.

(11) Weichman, M. L.; DeVine, J. A.; Levine, D. S.; Kim, J. B.; Neumark, D. M. Isomer-Specific Vibronic Structure of the 9-, 1-, and 2-Anthracenyl Radicals via Slow Photoelectron Velocity-Map Imaging. *Proc. Natl. Acad. Sci.* **2016**, *113* (7), 1698–1705. https://doi.org/10.1073/pnas.1520862113.

(12) DeVine, J. A.; Babin, M. C.; Blackford, K.; Neumark, D. M. High-Resolution Photoelectron Spectroscopy of the Pyridinide Isomers. *J. Chem. Phys.* **2019**, *151* (6), 064302. https://doi.org/10.1063/1.5115413.

(13) Rienstra-Kiracofe, J. C.; Tschumper, G. S.; Schaefer III, H. F.; Nandi, S.; Ellison, G. B. Atomic and Molecular Electron Affinities: Photoelectron Experiments and Theoretical Computations. *Chem. Rev.* **2002**, *102* (1), 231–282. https://doi.org/10.1021/cr990044u.

(14) Simons, J. Molecular Anions. *J. Phys. Chem. A* **2008**, *112* (29), 6401–6511. https://doi.org/10.1021/jp711490b.

(15) Lineberger, W. C. Once upon Anion: A Tale of Photodetachment. *Annu. Rev. Phys. Chem.* **2013**, *64* (1), 21–36. https://doi.org/10.1146/annurev-physchem-032511-143753.

(16) Zhu, G.-Z.; Wang, L.-S. High-Resolution Photoelectron Imaging and Resonant Photoelectron Spectroscopy *via* Noncovalently Bound Excited States of Cryogenically Cooled Anions. *Chem. Sci.* **2019**, *10* (41), 9409–9423. https://doi.org/10.1039/C9SC03861B.

(17) Reid, K. L. Photoelectron Angular Distributions. *Annu. Rev. Phys. Chem.* **2003**, *54* (1), 397–424. https://doi.org/10.1146/annurev.physchem.54.011002.103814.

(18) Sanov, A. Laboratory-Frame Photoelectron Angular Distributions in Anion Photodetachment: Insight into Electronic Structure and Intermolecular Interactions. *Annu. Rev. Phys. Chem.* **2014**, *65* (1), 341–363. https://doi.org/10.1146/annurev-physchem-040513-103656.

(19) Anstöter, C. S.; Dean, C. R.; Verlet, J. R. R. Sensitivity of Photoelectron Angular Distributions to Molecular Conformations of Anions. *J. Phys. Chem. Lett.* **2017**, *8* (10), 2268–2273. https://doi.org/10.1021/acs.jpclett.7b00726.

(20) Woodhouse, J. L.; Henley, A.; Parkes, M. A.; Fielding, H. H. Photoelectron Imaging and Quantum Chemistry Study of Phenolate, Difluorophenolate, and Dimethoxyphenolate Anions. *J. Phys. Chem. A* **2019**, *123* (13), 2709–2718. https://doi.org/10.1021/acs.jpca.8b11121.

(21) Anstöter, C. S.; Curchod, B. F. E.; Verlet, J. R. R. Geometric and Electronic Structure Probed along the Isomerisation Coordinate of a Photoactive Yellow Protein Chromophore. *Nat. Commun.* **2020**, *11* (1), 2827. https://doi.org/10.1038/s41467-020-16667-x.

(22) Bull, J. N.; Verlet, J. R. R. Observation and Ultrafast Dynamics of a Nonvalence Correlation-Bound State of an Anion. *Sci. Adv.* **2017**, *3*, e1603106.

(23) Liu, H. T.; Ning, C. G.; Huang, D. L.; Dau, P. D.; Wang, L. S. Observation of Mode-Specific Vibrational Autodetachment from Dipole-Bound States of Cold Anions. *Angew. Chem. - Int. Ed.* **2013**, *52* (34), 8976–8979. https://doi.org/10.1002/anie.201304695.

(24) Bull, J. N.; West, C. W.; Verlet, J. R. R. Ultrafast Dynamics of Formation and Autodetachment of a Dipole-Bound State in an Open-Shell π-Stacked Dimer Anion. *Chem Sci* **2016**, *7* (8), 5352–5361. https://doi.org/10.1039/C6SC01062H.

(25) Verlet, J. R. R.; Anstöter, C. S.; Bull, J. N.; Rogers, J. P. Role of Nonvalence States in the Ultrafast Dynamics of Isolated Anions. *J. Phys. Chem. A* **2020**, *124* (18), 3507–3519. https://doi.org/10.1021/acs.jpca.0c01260.

(26) Anstöter, C. S.; Mensa-Bonsu, G.; Nag, P.; Ranković, M.; Kumar T. P., R.; Boichenko, A. N.; Bochenkova, A. V.; Fedor, J.; Verlet, J. R. R. Mode-Specific Vibrational Autodetachment Following Excitation of Electronic Resonances by Electrons and Photons. *Phys. Rev. Lett.* **2020**, *124* (20), 203401. https://doi.org/10.1103/PhysRevLett.124.203401.

(27) Cooper, J.; Zare, R. N. Angular Distribution of Photoelectrons. *J. Chem. Phys.* **1968**, *48* (2), 942–943. https://doi.org/10.1063/1.1668742.

(28) Lv, Q.-Y.; Li, W.; Zhan, S.-Z.; Wang, J.-G.; Su, J.-Y.; Ding, A. Chemistry of Tetracyanoethylene (TCNE): From TCNE to Dicyanomethylacetate. *J. Organomet. Chem.* **2008**, *693* (7), 1155–1158. https://doi.org/10.1016/j.jorganchem.2008.01.044.

(29) Oana, C. M.; Krylov, A. I. Dyson Orbitals for Ionization from the Ground and Electronically Excited States within Equation-of-Motion Coupled-Cluster Formalism: Theory, Implementation, and Examples. *J. Chem. Phys.* **2007**, *127* (23), 234106. https://doi.org/10.1063/1.2805393.

(30) Oana, C. M.; Krylov, A. I. Cross Sections and Photoelectron Angular Distributions in Photodetachment from Negative Ions Using Equation-of-Motion Coupled-Cluster Dyson Orbitals. *J. Chem. Phys.* **2009**, *131* (12), 124114. https://doi.org/10.1063/1.3231143.

(31) Jordan, K. D.; Wang, F. Theory of Dipole-Bound Anions. *Annu. Rev. Phys. Chem.* **2003**, *54* (1), 367–396. https://doi.org/10.1146/annurev.physchem.54.011002.103851.

(32) Lykke, K. R.; Mead, R. D.; Lineberger, W. C. Observation of Dipole-Bound States of Negative Ions. *Phys. Rev. Lett.* **1984**, *52* (25), 2221–2224.

(33) Comita, P. B.; Brauman, J. I. Photodissociation Spectroscopy of the Negative Ion Dimer of Toluquinone. *J. Am. Chem. Soc.* **1987**, *109* (25), 7591–7597. https://doi.org/10.1021/ja00259a001.

(34) Huang, D.-L.; Liu, H.-T.; Ning, C.-G.; Zhu, G.-Z.; Wang, L.-S. Probing the Vibrational Spectroscopy of the Deprotonated Thymine Radical by Photodetachment and State-Selective Autodetachment Photoelectron Spectroscopy via Dipole-Bound States. *Chem. Sci.* **2015**, *6* (5), 3129–3138. https://doi.org/10.1039/C5SC00704F.

(35) Dessent, C. E. H.; Kim, J.; Johnson, M. A. Spectroscopic Observation of Vibrational Feshbach Resonances in Near-Threshold Photoexcitation of X−·CH3NO2 (X−=I− and Br−). *Faraday Discuss.* **2000**, *115* (0), 395–406. https://doi.org/10.1039/A909550K.

(36) Bull, J. N.; Buntine, J. T.; Scholz, M. S.; Carrascosa, E.; Giacomozzi, L.; Stockett, M. H.; Bieske, E. J. Photodetachment and Photoreactions of Substituted Naphthalene Anions in a Tandem Ion Mobility Spectrometer. *Faraday Discuss.* **2019**, *217* (0), 34–46. https://doi.org/10.1039/C8FD00217G.

(37) Huang, D.-L.; Liu, H.-T.; Ning, C.-G.; Dau, P. D.; Wang, L.-S. Resonant Photoelectron Imaging of Deprotonated Uracil Anion via Vibrational Levels of a Dipole-Bound Excited State. *Chem. Phys.* **2017**, *482*, 374–383. https://doi.org/10.1016/j.chemphys.2016.06.003.

(38) Simons, J. Propensity Rules for Vibration-Induced Electron Detachment of Anions. *J. Am. Chem. Soc.* **1981**, *103* (14), 3971–3976. https://doi.org/10.1021/ja00404a002.

(39) Zhu, G. Z.; Liu, Y.; Wang, L. S. Observation of Excited Quadrupole-Bound States in Cold Anions. *Phys. Rev. Lett.* **2017**, *119* (2), 1–5. https://doi.org/10.1103/PhysRevLett.119.023002.

(40) Stanley, L. H.; Anstöter, C. S.; Verlet, J. R. R. Resonances of the Anthracenyl Anion Probed by Frequency-Resolved Photoelectron Imaging of Collision-Induced Dissociated Anthracene Carboxylic Acid. *Chem. Sci.* **2017**, *8* (4), 3054–3061. https://doi.org/10.1039/c6sc05405f.

(41) Wiley, W. C.; McLaren, I. H. Time-of-Flight Mass Spectrometer with Improved Resolution. *Rev. Sci. Instrum.* **1955**, *26* (12), 1150–1157. https://doi.org/10.1063/1.1715212.

(42) Eppink, A. T. J. B.; Parker, D. H. Velocity Map Imaging of Ions and Electrons Using Electrostatic Lenses: Application in Photoelectron and Photofragment Ion Imaging of Molecular Oxygen. *Rev. Sci. Instrum.* **1997**, *68* (9), 3477–3484. https://doi.org/10.1063/1.1148310.

(43) Horke, D. A.; Roberts, G. M.; Lecointre, J.; Verlet, J. R. R. Velocity-Map Imaging at Low Extraction Fields. *Rev. Sci. Instrum.* **2012**, *83* (6), 063101. https://doi.org/10.1063/1.4724311.

(44) Roberts, G. M.; Nixon, J. L.; Lecointre, J.; Wrede, E.; Verlet, J. R. R. Toward Real-Time Charged-Particle Image Reconstruction Using Polar Onion-Peeling. *Rev. Sci. Instrum.* **2009**, *80* (5), 053104. https://doi.org/10.1063/1.3126527.

(45) Shao, Y.; Gan, Z.; Epifanovsky, E.; Gilbert, A. T. B.; Wormit, M.; Kussmann, J.; Lange, A. W.; Behn, A.; Deng, J.; Feng, X.; Ghosh, D.; Goldey, M.; Horn, P. R.; Jacobson, L. D.; Kaliman, I.; Khaliullin, R. Z.; Kuś, T.; Landau, A.; Liu, J.; Proynov, E. I.; Rhee, Y. M.; Richard, R. M.; Rohrdanz, M. A.; Steele, R. P.; Sundstrom, E. J.; Woodcock, H. L.; Zimmerman, P. M.; Zuev, D.; Albrecht, B.; Alguire, E.; Austin, B.; Beran, G. J. O.; Bernard, Y. A.; Berquist, E.; Brandhorst, K.; Bravaya, K. B.; Brown, S. T.; Casanova, D.; Chang, C.-M.; Chen, Y.; Chien, S. H.; Closser, K. D.; Crittenden, D. L.; Diedenhofen, M.; DiStasio, R. A.; Do, H.; Dutoi, A. D.; Edgar, R. G.; Fatehi, S.; Fusti-Molnar, L.; Ghysels, A.; Golubeva-Zadorozhnaya, A.; Gomes, J.; Hanson-Heine, M. W. D.; Harbach, P. H. P.; Hauser, A. W.; Hohenstein, E. G.; Holden, Z. C.; Jagau, T.-C.; Ji, H.; Kaduk, B.; Khistyaev, K.; Kim, J.; Kim, J.; King, R. A.; Klunzinger, P.; Kosenkov, D.; Kowalczyk, T.; Krauter, C. M.; Lao, K. U.; Laurent, A. D.; Lawler, K. V.; Levchenko, S. V.; Lin, C. Y.; Liu, F.; Livshits, E.; Lochan, R. C.; Luenser, A.; Manohar, P.; Manzer, S. F.; Mao, S.-P.; Mardirossian, N.; Marenich, A. V.; Maurer, S. A.; Mayhall, N. J.; Neuscamman, E.;

Oana, C. M.; Olivares-Amaya, R.; O'Neill, D. P.; Parkhill, J. A.; Perrine, T. M.; Peverati, R.; Prociuk, A.; Rehn, D. R.; Rosta, E.; Russ, N. J.; Sharada, S. M.; Sharma, S.; Small, D. W.; Sodt, A.; Stein, T.; Stück, D.; Su, Y.-C.; Thom, A. J. W.; Tsuchimochi, T.; Vanovschi, V.; Vogt, L.; Vydrov, O.; Wang, T.; Watson, M. A.; Wenzel, J.; White, A.; Williams, C. F.; Yang, J.; Yeganeh, S.; Yost, S. R.; You, Z.-Q.; Zhang, I. Y.; Zhang, X.; Zhao, Y.; Brooks, B. R.; Chan, G. K. L.; Chipman, D. M.; Cramer, C. J.; Goddard, W. A.; Gordon, M. S.; Hehre, W. J.; Klamt, A.; Schaefer, H. F.; Schmidt, M. W.; Sherrill, C. D.; Truhlar, D. G.; Warshel, A.; Xu, X.; Aspuru-Guzik, A.; Baer, R.; Bell, A. T.; Besley, N. A.; Chai, J.-D.; Dreuw, A.; Dunietz, B. D.; Furlani, T. R.; Gwaltney, S. R.; Hsu, C.-P.; Jung, Y.; Kong, J.; Lambrecht, D. S.; Liang, W.; Ochsenfeld, C.; Rassolov, V. A.; Slipchenko, L. V.; Subotnik, J. E.; Van Voorhis, T.; Herbert, J. M.; Krylov, A. I.; Gill, P. M. W.; Head-Gordon, M. Advances in Molecular Quantum Chemistry Contained in the Q-Chem 4 Program Package. *Mol. Phys.* **2015**, *113* (2), 184–215. https://doi.org/10.1080/00268976.2014.952696.

(46) Chai, J.-D.; Head-Gordon, M. Long-Range Corrected Hybrid Density Functionals with Damped Atom–Atom Dispersion Corrections. *Phys. Chem. Chem. Phys.* **2008**, *10* (44), 6615. https://doi.org/10.1039/b810189b.

(47) Dunning, T. H. Gaussian Basis Sets for Use in Correlated Molecular Calculations. I. The Atoms Boron through Neon and Hydrogen. *J. Chem. Phys.* **1989**, *90* (2), 1007–1023. https://doi.org/10.1063/1.456153.

(48) Mozhayskiy, V.; Krylov, A. I. *EzSpectrum v3.0*; http://iopenshell.usc.edu/downloads; http://iopenshell.usc.edu/downloads.

(49) Krylov, A. I. Equation-of-Motion Coupled-Cluster Methods for Open-Shell and Electronically Excited Species: The Hitchhiker's Guide to Fock Space. *Annu. Rev. Phys. Chem.* **2008**, *59*, 433–462. https://doi.org/10.1146/annurev.physchem.59.032607.093602.

(50) Gozem, S.; Krylov, A. I. *EzDyson V4*; http://iopenshell.usc.edu/downloads/ezdyson; http://iopenshell.usc.edu/downloads/ezdyson.

(51) Bravaya, K. B.; Zuev, D.; Epifanovsky, E.; Krylov, A. I. Complex-Scaled Equation-of-Motion Coupled-Cluster Method with Single and Double Substitutions for Autoionizing Excited States: Theory, Implementation, and Examples. *J. Chem. Phys.* **2013**, *138* (12), 124106. https://doi.org/10.1063/1.4795750.

(52) Skurski, P.; Gutowski, M.; Simons, J. How to Choose a One-electron Basis Set to Reliably Describe a Dipole-bound Anion. *Int. J. Quantum Chem.* **2000**, *80* (4–5), 1024–1038.

(53) Voora, V. K.; Kairalapova, A.; Sommerfeld, T.; Jordan, K. D. Theoretical Approaches for Treating Non-Valence Correlation-Bound Anions. *J. Chem. Phys.* **2017**, *147* (21), 214114. https://doi.org/10.1063/1.4991497.